Effects of Structure Vibrations and Noise on Passenger Bus Seat Ride Comfort

UDC:623.3.015.5/.6
Original scientific paper https://doi.org/10.46793/adeletters.2026.5.2.2

Vu Hai Quan[1], Nguyen Duc Hai[1], Nguyen Anh Ngoc[1*], Kirill Evgenievich Karpukhin[2], Nguyen Trong Duc[1,3]

[1]School of Mechanical and Automotive Engineering, Hanoi University of Industry (HaUI), Hanoi 100000, Vietnam
[2]NAMI Russian State Scientific Research Center, Moscow, Russia
[3]Moscow Automobile and Road Construction State Technical University, Russia

Abstract:
Noise, vibration, and harshness (NVH) are critical parameters influencing passenger comfort and overall satisfaction during bus travel. Despite some improvements, domestic bus manufacturers in Vietnam remain dependent on imported components, particularly in interior noise control and ride comfort. This study investigates the NVH characteristics of the Thaco Garden TB79S bus, with an emphasis on the role of the body structure in operational comfort. Numerical simulations were performed in MATLAB/Simulink and Hypermesh software under two representative road profiles common in Vietnam, a sine wave and a Class C random profile ISO 8608:2016 at 60 km/h. Results indicate that the maximum cabin sound pressure level (SPL) under sinusoidal excitation reached 192.04 dB, with resonances at 77 Hz and 99 Hz, while under random excitation the SPL varied between 80 and 138 dB. These SPL values should be regarded as relative references rather than actual levels perceived by occupants, since the model simplified other factors such as acoustic absorption, aerodynamic noise, tire noise, and engine noise. Meanwhile, ride comfort at the driver's seat was evaluated according to ISO 2631-1:1997/Amd 1:2010, with a_{rms} values of 0.112 and 0.813 m/s², clearly reflecting the influence of road surface irregularities on driver perception.

ARTICLE HISTORY
Received: 21 December 2025
Revised: 13 April 2026
Accepted: 23 April 2026
Published: 22 June 2026

KEYWORDS
Noise, Vibration, Natural vibration, Harshness, NVH, FEM, Bus

1. INTRODUCTION

In recent years, the automotive industry worldwide, including Vietnam, has increasingly focused on reducing emissions and developing environmentally friendly vehicles. In this context, electric and hybrid vehicles have become a major focus of research and development investment by manufacturers. However, changes in the powertrain architecture, particularly the reduction or elimination of internal combustion engines, significantly alter vehicle dynamics and vibration characteristics, thereby highlighting issues related to Noise, Vibration, and Harshness (NVH). Particularly in Vietnam, where road surface conditions are diverse, and transportation infrastructure quality remains inconsistent, and amid humid tropical environmental factors, vehicle vibration and acoustic responses exhibit significant variability. These excitations directly impact occupant health, safety, and perceived comfort [1]. However, domestic NVH research remains limited, with most studies relying solely on experimental data or analyzing isolated subsystems. The absence of an integrated computational framework that couples vehicle dynamics, structural finite element

*CONTACT: Nguyen Anh Ngoc, e-mail: ngocnguyencnoto@haui.edu.vn

modeling, and acoustic simulation limits the ability to accurately and efficiently assess the overall NVH behavior of vehicles under realistic conditions.

Noise, vibration, and harshness generated from the vehicle chassis have a direct impact on passenger comfort and health. During vehicle operation, these factors often cause discomfort and reduce overall user satisfaction. Prolonged exposure to vibration and noise may lead to fatigue, increased stress on the nervous system, reduced concentration, and, in some cases, hearing impairment. These effects are particularly significant for passenger vehicles, where ride comfort and cabin acoustic quality are key indicators of perceived vehicle quality. Therefore, automotive manufacturers worldwide are increasingly focusing on optimizing NVH performance as a critical objective in the development of new vehicle models.

The main objective of this study is to develop a computational model for evaluating vehicle vibration and interior noise. Specifically, a half-vehicle dynamic model is integrated with a finite element model (FEM) of the vehicle body structure and an interior acoustic model of the passenger cabin. This integrated approach enables coupled vibro-acoustic analysis to assess ride comfort and cabin noise levels, particularly at the driver's ear position. This is due to the transmission of noise to the occupant's ears through the vehicle's structural pathways and through the surrounding air [2]. Compared with conventional experimental methods, which are often costly and difficult to implement under limited research conditions, the proposed simulation framework provides a more practical, reproducible, and efficient alternative while still yielding meaningful engineering insights.

The study investigates road-induced excitations representative of Vietnamese driving conditions and their impact on noise generation inside the cabin. Two road surface profiles are considered: a sinusoidal profile and a Class C random road with stochastic amplitude variations defined by ISO 8608:2016 [3]. Two types of dynamic analyses are conducted: harmonic response analysis and transient response analysis. The results demonstrate a direct relationship between sound pressure fluctuations and excitation frequency generated by the road profile. Furthermore, resonance phenomena are observed between the varying excitation frequencies, the structural natural modes of the vehicle body, and the acoustic modes of the cabin. These interactions are evaluated against standard human hearing thresholds to quantify their perceptual significance.

In addition, a 15 s transient noise analysis was performed while the vehicle traveled over the Class C random road surface. Key acoustic quantities, including sound pressure (SP) and sound pressure level (SPL), were monitored over time to characterize the driver's auditory perception of noise. The Fast Fourier Transform (FFT) technique [4] was employed to decompose the SPL distribution into distinct frequency components, thereby identifying dominant frequency bands that contributed to subjective noise perception. Finally, ride comfort at the driver's position was assessed in accordance with ISO 2631-1:1997/Amd 1:2010 [5], which provided a quantitative basis for structural and suspension optimization to enhance overall NVH quality and occupant satisfaction.

2. RELATED WORKS

Many studies have applied FEM to analyze vibrations and acoustics, and to optimize vehicle structures to improve the NVH quality of automobiles. Research [6] showed that optimizing the shape and material of the body can increase the first oscillation frequency by about 14%, reduce the displacement by 36.8%, and reduce the mass by 19%, thereby reducing the transmission of vibration into the cabin. In research [7-10] also showed that identifying the panels that contribute the most to low-frequency noise and optimising the stiffness or thickness of the panels can reduce the sound pressure level in the cabin by 3-8 dB; for buses in particular, changing the roof frame stiffness can reduce the noise level in the interior compartment by about 60% [8-10].

Studies that combine computational fluid dynamics-finite element modeling (CFD–FEM) with advanced methods such as isogeometric analysis (IGA) have also been developed. Wang et al. [11] showed that underbody airflow increases cabin SPL in the low- and mid-frequency ranges and can be significantly reduced by changing the material or floor thickness. In [12], it was shown that the IGA method achieved higher accuracy than the traditional FEM, with a frequency error below 1% and fewer degrees of freedom.

Several experimental studies that combined vibration acoustic path analysis (TPA) also showed the important role of structural and suspension design. Research [13] demonstrated that optimizing vibration transmission points can significantly reduce cabin noise levels. In addition, the group of authors led by Frank et al. [14] achieved reductions of up to 50% in floor vibration and 3 dBA in cabin noise after improving the suspension and chassis system. Research [15] determined that forced modes from the powertrain are the main noise source, and the solution requires increasing the damping coefficient at key locations.

For electric vehicles/battery electric vehicles (EV/BEV), due to the lack of masking from the engine, road-tire and wind noise become the dominant sources. Research [16, 17] argued that the NVH model needs to be adjusted to suit the vibration-acoustic characteristics of electric vehicles and could improve noise levels by up to 5dBA at low speeds. In research [18], the impact of each floor panel on the sound pressure at the driver's position was evaluated by optimizing the floor panel structure, resulting in a 2-3 dB noise reduction and a significant improvement in resonance. In some previous studies [19, 20], the authors have evaluated the vibration of passenger cars using a magnetorheological fluid damper and investigated the influence of the vehicle body panel and the acoustic cavity on the distribution of sound pressure levels inside the passenger compartment, particularly at seating positions. However, the body panel constitutes only a subset of the vehicle's overall structural framework. Therefore, the present study extends this work by incorporating the combined effects of the body panel, chassis frame, floor structure, and the internal acoustic cavity.

3. THEORETICAL FOUNDATION FOR RESEARCH ON NOISE AND VIBRATION IN TRANSPORT VEHICLES

3.1. Sound Pressure

Negative pressure, or sound pressure, is the local pressure difference from the average atmospheric pressure caused by a sound wave. Negative pressure in the air can be measured using a microphone, and in water using a hydrophone. The SI unit for negative pressure is pascal (Pa).

3.2. Sound Pressure Level

SPL is a measure of the sound pressure level relative to a fixed reference level. It is measured in decibels (dB) and indicates the strength of sound that the human ear can perceive. The commonly used reference level (p_{ref}) is 20 µPa.

$$SPL=10\log_{10}\left(p_{rms}^{2}/p_{ref}^{2}\right) \tag{1}$$

$$p_{rms}=\frac{p_{max}^{2}}{2} \tag{2}$$

Where are: p_{rms} - is root mean square sound pressure; p_{max} - is the maximum sound pressure.

3.3. Fourier Transform

The Fourier transform is an integral transformation that takes a function as input and produces another function that describes the extent to which different frequencies are present in the original function. It enables conversion of a signal from the time domain to the frequency domain, allowing detailed analysis of the sound's frequency structure.

$$X(f)=\int_{-\infty}^{\infty}x(t)e^{-j2\pi ft}dt \tag{3}$$

Where are: $X(f)$ - is the amplitude of the signal at frequency; $x(t)$ - is a signal in the time domain.

3.4. Normal Modes Analysis

The natural frequencies of a system depend solely on the stiffness of the structure and the mass associated with it, including the vehicle’s weight and other boundary conditions. The governing equation describing the vibration of the vehicle body structure is:

$$M\ddot{x}+C\dot{x}+Kx=f(t) \tag{4}$$

where are: M - is the mass matrix of the structure; K is the stiffness matrix of the structure; C - is a damping matrix; $\ddot{x}$ - is the acceleration vector of the nodes; $\dot{x}$ - is the velocity vector of the nodes; $f(t)$ - is a vector of time-varying loads.

$$M\ddot{x}+Kx=0 \tag{5}$$

The solution of this equation can be evaluated if they have a conditioning solution in the form of:

$$x=\phi\sin(\omega t) \tag{6}$$

where are: ϕ - is denotes the mode shape or eigenvector; ω - is the natural frequency.

$$-\omega^{2}M\phi\sin(\omega t)+K\phi\sin(\omega t)=0 \tag{7}$$

$$(K-\omega^{2}M)\phi=0 \tag{8}$$

Reformulated using the eigenvalue definition $\lambda=\omega^{2}$.

$$(K-\lambda M)\phi=0 \tag{9}$$

3.5. Normal Modes Analysis

The model analysis involves solving the eigenvalue problem to obtain eigenvalues λ_i and eigenvectors A:

$$u = Ade^{i\Omega t} \quad (10)$$

where are: u - is the displacement vector; ω - is the amplitude coefficient; i is an imaginary unit (i = $\sqrt{-1}$); Ω - is angular frequency.

The undamped equation of motion is then transformed into modal coordinates using the individual eigenvectors:

$$\left[- \Omega A^T MA + A^T KA\right] de^{i\Omega t} = A^T fe^{i\Omega t} \quad (11)$$

where are: $A^T MA$ and $A^T KA$ - are the mass and stiffness matrices, respectively, which are diagonal,

$$\left[-\Omega^2 m_i + i\Omega C_i + k_i\right] de^{i\Omega t} = f_i e^{i\Omega t} \quad (12)$$

where are: m_i - is modal mass; c_i - is modal damping; k_i - is modal stiffness.

The three damping values defined by the $g_i\left(f_i^{freq}\right)$ approach are interrelated via the following three resonance equations:

$$G = \zeta_i = \frac{c_i}{c_{cr}} = \frac{g_i}{2} \quad (13)$$

$$CRIT = C_{Cr} = 2m_i\omega_i \quad (14)$$

$$Q = Q_i = \frac{1}{2\zeta_i} = \frac{1}{g_i} \quad (15)$$

where are: $\zeta_i = {}^{c_i}/_{2m_i w_i}$ - is the modal damping ratio; $w_i^2 = {}^{k_i}/_{m_i}$ - is the modal eigenvalue; c_{cr} - is the critical damping coefficient; g_i - is the modal loss factor; Q_i - is a quality factor.

Modal damping is incorporated into the complex stiffness matrix as structural damping when PARAM, KDAMP and -1 are used. Subsequently, the uncoupled equation becomes:

$$\left[- \Omega^2 m_i + \left(1 + ig(\Omega)\right)k_i\right] de^{i\Omega t} = f_i e^{i\Omega t} \quad (16)$$

3.6. Model Transient Response Analysis

The transient response analysis involves calculating the structural reactions by solving the equations of motion below, subject to initial conditions represented in matrix form:

$$M\ddot{u} + B\dot{u} + ku = f(t) \quad (17)$$

$$u(t=0) = u_0;\ \dot{u}(t=0) = \dot{u}_0;\ \ddot{u}(t=0) = \ddot{u}_0 \quad (18)$$

where are: $f(t)$ - is the time-dependent load; M - is the mass matrix; B - is the damping matrix; k - is the stiffness matrix; $\ddot{u}$, $\dot{u}$, and u-represent displacement; u_0, $\dot{u}_0$, $\ddot{u}_0$-are velocity and acceleration as functions of time, respectively, denote the initial conditions of the problem.

The analysis yields eigenvalues and their corresponding eigenvectors. The state vector $\lambda_i = w_i^2 A = A_i$ can be expressed as the scalar product of the eigenvectors AAA and the modal response v:

$$u=Av \quad (19)$$

The undamped equation of motion is then transformed into modal coordinates by using the individual eigenvectors:

$$A^T MA\ddot{v} + A^T kAv = A^T f \quad (20)$$

where are: $A^T MA$ - the mass matrix and $A^T MA$ the stiffness matrix are diagonal matrices; f - is the excitation force vector.

This way, the system equation is reduced to a set of uncoupled equations for the components of v that can be easily solved. The inclusion of damping yields:

$$A^T MA\ddot{v} + A^T CA\dot{v} + A^T kAv = A^T f \quad (21)$$

where: $A^T CA$ - is a non-diagonal matrix.

3.7. Ride Comfort Index According to ISO 2631-1

ISO 2631-1/Amd 1:2010 [5] provides a standard for evaluating ride comfort based on the root-mean-square (RMS) value of acceleration, denoted as a_{rms}. The level of comfort is based on the a_{rms} index shown in Table 1. The acceleration data, once extracted, is processed to determine the RMS index as follows:

$$a_{rms} = \left[\frac{1}{T}\int_0^T a_w^2(t)\,dt\right]^{\frac{1}{2}} \quad (22)$$

where are: T - is the evaluation time period; $a_w(t)$ - is weighted acceleration over time.

Table 1. Level of comfort as defined by ISO 2631-1:1997/Amd 1:2010

a_{rms} (m/s²)	Ride comfort
< 0.315	Not uncomfortable
0.315 ÷ 0.63	Slightly uncomfortable
0.5 ÷ 1.0	Moderately uncomfortable
0.8 ÷ 1.6	Uncomfortable
1.25 ÷ 2.5	Very uncomfortable
> 2	Extremely uncomfortable

4. MATERIALS AND METHODS

An integrated numerical approach is adopted to evaluate vehicle ride comfort and interior noise. The methodology combines vehicle dynamic modeling, structural finite element analysis, and cabin acoustic simulation within a unified vibro-acoustic framework

A half-vehicle dynamic model was developed to describe the vehicle's vertical and inclined motion. Road surface irregularities are modeled as vertical displacement excitations acting on the wheels, serving as the primary vibration inputs.

The vehicle body was modeled using the finite element method to capture its structural dynamic characteristics. Modal analysis is performed to obtain natural frequencies and mode shapes within the NVH-relevant frequency range.

The passenger cabin was represented as an enclosed acoustic cavity. The acoustic response inside the cabin is calculated considering appropriate boundary conditions and damping to simulate sound propagation and absorption.

Structural vibrations of the vehicle body are coupled with the cabin acoustic model through shared interfaces. This coupling enables the prediction of interior sound pressure levels induced by structural excitation.

Ride comfort was evaluated using frequency-weighted RMS acceleration in accordance with ISO 2631-1:1997/Amd 1:2010. The W_k frequency weighting curve is applied to vertical acceleration signals at the driver’s seat and ear position. Interior noise is assessed based on sound pressure levels at the driver’s ear.

Despite its simplifications, the half-vehicle vertical model depicted in Fig. 1 still provides a consistent and efficient framework for comparative NVH analysis, which is the focus of the present study.

5. DEVELOPMENT OF THE SIMULATION MODEL

5.1. Half Vehicle Vibration Model

A half-vehicle suspension model was developed using MATLAB/Simulink to simulate chassis excitation and evaluate the vibration response and ride comfort at the driver's seat. In this study, a vibration model was constructed by modeling the air spring elements as equivalent spring-damped systems. The tire and air spring elastic elements were represented by spring elements with equivalent stiffness and damping coefficients.

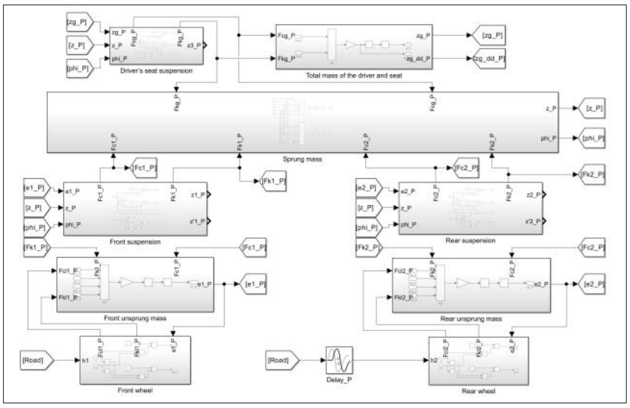

Fig. 1. Half vehicle vibration Simulink model

Modeling assumptions for the half vehicle suspension model of a 29-seater bus:

- The road surface profile is the only source of excitation.
- The sprung mass, front axle, and rear axle are modeled as rigid bodies with lumped mass.
- The tires remain in continuous contact with the road surface; the vehicle moves in a straight line on a non-deformable road at a constant speed.
- All elastic and damping elements are assumed to be linear.
- The stiffness and damping coefficients are considered constant.
- Vehicle vibrations considered for ride comfort evaluation are vertical motions only.

MATLAB/Simulink is used to generate excitation amplitudes based on two types of input profiles: sine-wave profiles and random road profiles of class C, in accordance with ISO 8608:2016. The corresponding excitation forces acting on the vehicle's front and rear axles are computed over the simulation time period.

5.2. Finite Element Model

This study uses a FEM of the Thaco Garden TB79S bus body frame, developed using HyperMesh software, combined with a cabin acoustic model to study the interior noise and evaluate the impact of noise and vibration on passengers, focusing on the driver's position.

The boundary conditions of the problem are determined based on the excitation force transmitted from the road surface through the suspension system to the body frame, while ignoring the influence of other excitation sources. Given the limitations of existing computational resources, the elements are created with appropriate numbers and sizes to ensure the problem can be solved. The mesh size of the finite elements and the 3D model developed in the numerical environment are presented in Table 2 and Figs. 2, 3, 4, and 5. The material properties are provided in Tables 3 and 4.

Table 2. FE size of the model in HyperMesh OptiStruct

Part	Element size (mm)
Floor	30
Shells	30
Car frame	10
Windshield	10
Window	10
Cabin acoustic cavity	40

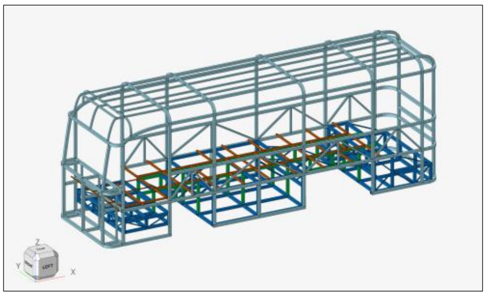

Fig. 2. FEM of the structural frame

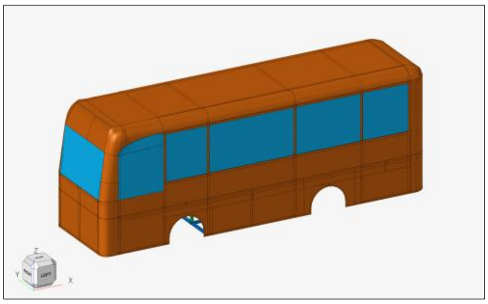

Fig. 3. FEM of the combined frame–body assembly

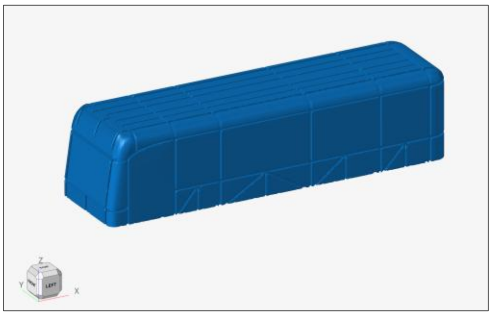

Fig. 4. FEM of acoustic cavity

Fig. 5. The excitation load of the FEM

Table 3. Material specifications of the model

Material	Young's Modulus (GPA)	Poisson's ratio	Density (kg/m^3)
Steel	210	0.3	7850
Glass	70	0.3	7850
Air	-	-	1125

Table 4. Thickness of components in the FEM

Part	Material	Thickness (mm)
Floor	Steel	1.5
Shells	Steel	0.7
Car frame	Steel	3
Windshield	Glass	7
Window	Glass	5

Assumptions of the dynamic finite element model for the passenger car frame and body:

- The frame and vehicle body are modeled as an absolutely rigid body.
- The excitation vibration is represented as a vertical force.
- Vibrations and excitation sources caused by the engine and drivetrain are neglected.

The material properties and thicknesses of the components in the FEM are presented in Tables 3 and 4, respectively. The chassis, floor, and body structure primarily use steel, while the windscreen and doors are modeled with glass at the proposed thicknesses.

In this setup, the excitation load used in the model is configured from the suspension system with load levels depending on the road-profile transition and the type of simulation problem. It is placed in the next 4 positions of the passenger car body system. The load has a frequency that varies from 1 to 200 Hz, ignoring time delay and phase.

6. SIMULATION RESULTS AND DISCUSSION

It should be noted that the SPL values presented in this section are relative FEM results obtained under simplified assumptions and do not represent actual sound pressure levels inside a real vehicle cabin.

6.1. Natural Vibration Analysis of the Vehicle Frame and Body

The simulation problem is modeled as the free vibration of a monolithic structure, with damping effects assumed negligible and external forces set to zero during the analysis. In several NVH studies, sound pressure is typically evaluated under engine excitation, with dominant vibration frequencies around 50 Hz [21], or under road-induced inputs, with vibration frequency spectra ranging from 0 to 100 Hz [22]. Vibrators capable of generating vibrations with frequencies ranging from 20 to 200 Hz are integrated into driving simulators [23]. In this study, the excitation source is modeled as a rough road surface, with an extended frequency range of 0 to 200 Hz to comprehensively represent real-world effects, as shown in Fig. 6.

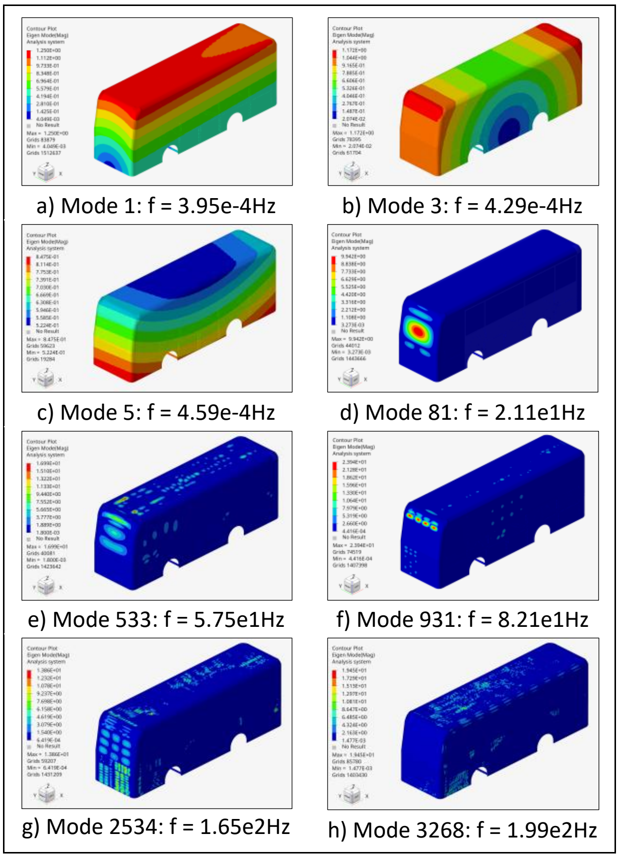

a) Mode 1: f = 3.95e-4Hz
b) Mode 3: f = 4.29e-4Hz
c) Mode 5: f = 4.59e-4Hz
d) Mode 81: f = 2.11e1Hz
e) Mode 533: f = 5.75e1Hz
f) Mode 931: f = 8.21e1Hz
g) Mode 2534: f = 1.65e2Hz
h) Mode 3268: f = 1.99e2Hz

Fig. 6. Sample results of natural vibration modes of the bus frame–body assembly obtained from eigenvalue analysis

From Table 5, the analysis of the natural vibrations of the finite element model of the passenger car body frame yielded the natural frequencies and corresponding mode shapes. The first six oscillation modes will have frequencies approximately 0, which is correct under the constraint condition because the model is not constrained by any degrees of freedom. The natural frequencies of the vehicle body lie within the 200Hz frequency range. For each vibration mode, the system exhibits a specific response, allowing the prediction of system behavior when external forces act at frequencies coinciding with its natural frequencies. Low-frequency stimuli are highly sensitive to low-frequency oscillation modes, which can cause significant vibrations and noise inside the vehicle, affecting driver comfort [24].

Table 5. Simulation results of the vibration frequency of the finite element model of the car body and frame

Mode	1	2	3
Frequency (Hz)	3.95e-4	4.21e4	4.29e-4
Mode	4	5	6
Frequency (Hz)	4.44e-4	4.59e-4	4.72e-4
Mode	7	8	9
Frequency (Hz)	4.85	4.97	5.58
Mode	10	11	12
Frequency (Hz)	5.67	5.92	6.67
Mode	13	14	15
Frequency (Hz)	7.05	7.17	7.44

6.2. Natural Vibration Analysis of the Cabin Acoustics

This study employs an acoustic model to analyze the natural vibration frequencies within the cabin compartment. The model is extracted separately from the overall 3D frame and body structure, where external structural components are omitted, retaining only the acoustic volume of the cabin to focus on the resonance characteristics inside the enclosed space.

The natural frequency range of the cabin acoustic model is established similarly to the modal analysis performed on the vehicle frame and body structure. Some simulation results of natural oscillations obtained from the cabin acoustic model are shown in Fig. 7. The corresponding frequency values of these modes are described in Table 6.

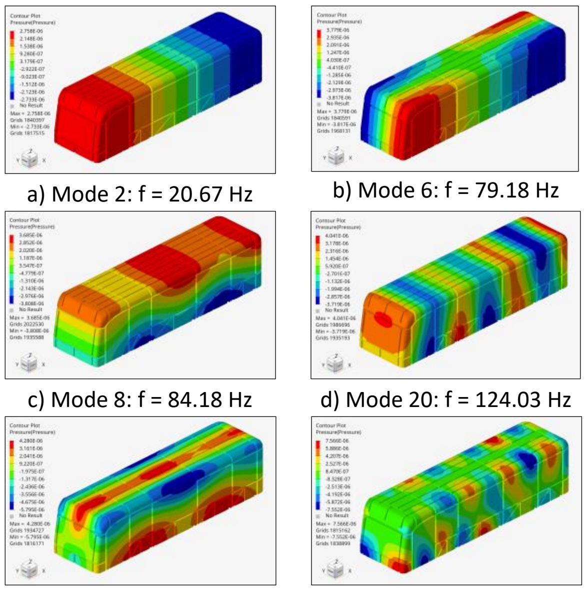

a) Mode 2: f = 20.67 Hz
b) Mode 6: f = 79.18 Hz
c) Mode 8: f = 84.18 Hz
d) Mode 20: f = 124.03 Hz
e) Mode 41: f = 174.67 Hz
f) Mode 59: f = 198.15 Hz

Fig. 7. Sample results of natural vibration modes of the cabin acoustics obtained from eigenvalue analysis

Table 6. Simulation results of the vibration frequency of the finite element model of the cabin acoustic

Mode	1	2	3
Frequency (Hz)	1.32e-5	20.66	41.26
Mode	4	5	6
Frequency (Hz)	61.89	76.14	79.18
Mode	7	8	9
Frequency (Hz)	82.07	84.18	86.84
Mode	10	11	12
Frequency (Hz)	86.87	93.83	98.44
Mode	13	14	15
Frequency (Hz)	102.65	105.39	112.27

In the frequency range from 0-200 Hz, the study identified 59 natural oscillation modes of the air mass inside the vehicle. The first natural oscillation frequencies found are summarised in Table 6, and some typical oscillation modes are shown in Fig. 7. The natural oscillation modes are represented through the quantity of pressure in the passenger compartment. For each specific oscillation mode, the distribution of air pressure inside will be different. The results obtained allow us to determine the area with higher air pressure as well as the pressure distribution corresponding to each oscillation mode. The second oscillation mode has a high negative pressure level at the driver's position, and the second oscillation mode has a high negative pressure level at the rear passenger position.

Within the 0–200 Hz frequency range, 59 vibration modes of the air volume have been identified. These modes correspond to the sound pressure levels inside the cabin, including localized regions of maximum sound pressure and the surrounding air pressure distribution. Each vibration mode represents a distinct spatial distribution of air pressure.

6.3. Analysis of Noise at Seating Positions Under Vehicle Operation on a Sine-Wave Road Profile

In this analysis, the amplitude of the excitation force is held constant across the studied frequency range. The sound pressure level at the driver's position is calculated by summing the responses at each excitation frequency, reflecting the real scenario in which the vehicle passes over speed bumps with uniform shape and spacing. In this research, a road surface detailed in Eq. 23 is selected for both the front and rear wheels at a vehicle speed of 60 km/h to simulate the vehicle's vibration and noise over a sine wave road profile. The forces exerted on the vehicle chassis are illustrated in Fig. 8. The maximum loads at the two axle locations are detailed in Table 7.

$$h=10\sin(34\pi t) \quad (23)$$

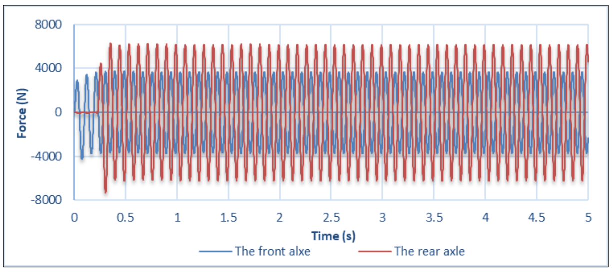

Fig. 8. Force applied to the front axle and the rear axle

Table 7. Maximum force values for the sine wave profile

Speed (m/s)	Maximum front axle force (N)	Maximum rear axle force (N)
60	3758.73	6313.71

Fig. 9 highlights clear disparities in SPL distribution across different seating positions, reflecting the acoustically non-uniform nature of the vehicle cabin. The rear seat exhibits the highest SPL peak at 192.04 dB and the lowest minimum at 74.08 dB, indicating a wide fluctuation range likely due to sound reflections and acoustic resonance occurring near the vehicle's rear boundary. In contrast, the center seat shows the most stable acoustic behavior, with the lowest SPL peak at 190.41 dB and the highest minimum at 92.59 dB. This suggests reduced sensitivity to localized noise sources and improved insulation performance, likely due to its equidistant placement relative to primary vibration inputs. At the driver's seat, the SPL peak of 191.83 dB is only marginally lower than that of the rear seat, while the minimum value of 80.33 dB indicates a moderate fluctuation range. These characteristics are consistent with its proximity to the front suspension system, which serves as a significant path for vibration transmission. Given that this is the operator's primary working position throughout vehicle operation, greater demands are placed on acoustic consistency and ride comfort. The maximum and minimum SPL values observed at the three locations are presented in Table 8. These findings underscore the necessity of optimizing sound insulation and noise mitigation specifically for the driver's zone to enhance comfort and maintain driver concentration during prolonged operation.

The study uses the maximum excitation force values obtained at various vehicle speeds to determine the excitation force amplitude in the sound pressure analysis.

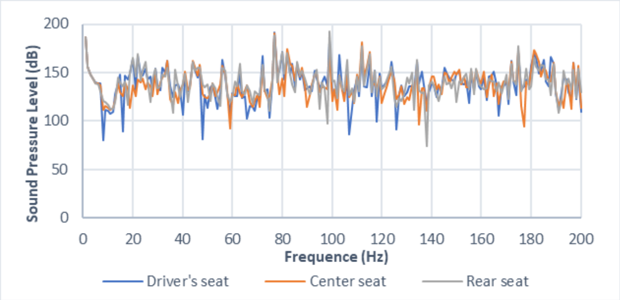

Fig. 9. SPL at three seating positions over a sine wave profile

Table 8. Limits of SPL with sine wave input

Survey positions	Maximum SPL (dB)	Minimum SPL (dB)
Driver's seat	191.83	80.33
Center seat	190.41	92.59
Rear seat	192.04	74.08

The survey results indicate that the highest maximum sound pressure level was recorded at the rear seat, 192.04 dB, followed by the driver's seat, 191.83 dB, and the lowest at the middle seat, 190.41 dB. Conversely, the highest minimum sound pressure level appeared at the middle seat, 92.59 dB, while the rear seat registered the lowest value, 74.08 dB. This suggests that the middle seat experiences less fluctuation in sound, whereas the rear seat exhibits the greatest variation in sound levels.

From Table 9, it is observed that resonance occurs at most points with high sound pressure levels, including the point with the maximum sound pressure. This resonance phenomenon happens when the excitation force frequency approaches the natural frequency of the air volume or the natural frequency of the frame–body structure [25]. This aligns perfectly with the actual physical behavior.

Table 9. Comparison of resonant frequencies

Max SPL (dB)	Frequency at SPL peaks (Hz)	Natural frequency of the cabin acoustics (Hz)	Natural frequency of the frame-body (Hz)
166.91	72	-	72.00
191.83	77	76.94	77.05
170.78	80	79.56	80.04
168.64	82	82.07	81.99
172.93	112	112.26	112.02
170.50	175	174.67	175.04
169.65	181	180.31	180.002
…	…	…	…

6.4. Analysis of Noise at Seating Positions Under Vehicle Motion on Uneven Road Surfaces

In reality, a vehicle is subjected to various types of road surface profiles that are continuously and irregularly distributed. Consequently, the excitation force from the road to the vehicle body varies at different moments. The sound pressure level inside the cabin correspondingly evolves throughout the vehicle's operation on the road. This study focuses on the analysis of a Class C random road profile according to ISO 8608:2016 [2], with a vehicle speed of 60 km/h. This road profile and the corresponding chassis excitation forces applied to the simulation are illustrated in Figs. 10 and 11.

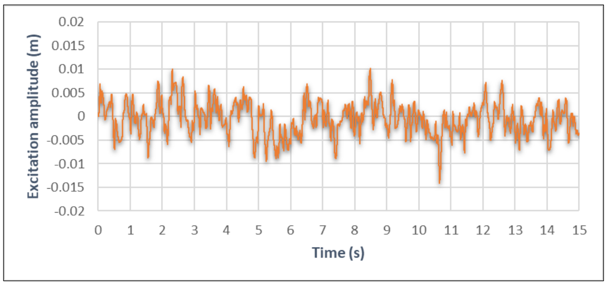

Fig. 10. Class C random road profile excitation based on ISO 8608

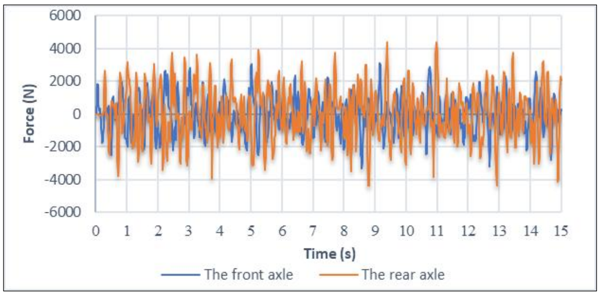

Fig. 11. Force applied to the front axle and the rear axle

Analysis of the results from Fig. 12 indicates that the driver's seat experiences the highest SPL, measured at 138.61 dB, along with pronounced acoustic fluctuations. This suggests a significant impact from road-induced vibrational noise transmitted through the vehicle structure. The minimum SPL at this location is 52.51 dB, which falls within the midrange threshold but indicates a wide fluctuation range, potentially contributing to increased auditory fatigue during prolonged exposure. The center seat, located equidistantly from both front and rear suspension components, demonstrates the most stable acoustic conditions. This is evidenced by the narrowest fluctuation range, indicating reduced influence from structural vibration sources and better interior acoustic performance. The rear seat registers a peak SPL of

138.30 dB and a minimum of 51.08 dB, revealing a wide amplitude range possibly caused by resonant or reflective effects within the rear cabin area. The range of SPL values, including both maximum and minimum levels recorded at the three locations, is detailed in Table 10. These phenomena may result from sound wave interactions at the vehicle's rear boundary, amplifying local pres-sure levels. Overall, both the driver's and rear seats exhibit greater acoustic variability, which may lead to discomfort under extended exposure. Notably, the driver's position requires prioritized noise-reduction measures due to the operational demands of continuous presence and sustained concentration during vehicle use.

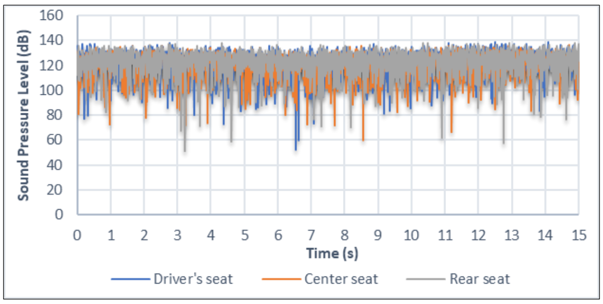

Fig. 12. SPL at three seating positions over a class C random road profile

Table 10. Limits of the SPL class C random surface

Survey positions	Maximum SPL (dB)	Minimum SPL (dB)
Driver's seat	138.61	52.51
Center seat	136.53	60.37
Rear seat	138.30	51.08

In practical applications, signals such as sound, electromagnetic waves, and light are often analyzed in the frequency domain. Frequency-domain analysis of interior noise enables identification of dominant frequency components that contribute to the overall sound pressure level within a given bandwidth. Among all seating positions, the driver's position requires special attention in noise assessment due to prolonged, continuous exposure to vibration and acoustic stimuli during vehicle operation. This unique condition arises because the driver is the only occupant required to maintain a fixed seated posture throughout the driving period. To examine the spectral characteristics of cabin noise at the driver's position, the fast Fourier transform (FFT) method is employed to convert the recorded time-domain acoustic signals into the frequency domain. The frequency-domain SPL at this cabin position is illustrated in Fig. 13.

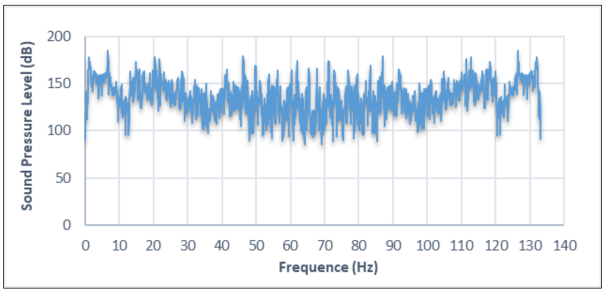

Fig. 13. SPL at three seating positions over a class C random road profile

The frequency-domain results indicate that the noise at the driver's position consists of sound signals with frequencies ranging from 1 to 133 Hz. Most of the frequencies contributing to the sound pressure level fall between 100 and 150 Hz. Additionally, the spectrum shows elevated noise levels at 1.49 Hz, 6.71 Hz, 21.81 Hz, 46.35 Hz, 62.04 Hz, 87.04 Hz, 92.12 Hz, 113.47 Hz, 118.42 Hz, 126.62 Hz, 131.77 Hz, and 132.29 Hz. These frequencies represent the primary contributors to the high sound pressure levels within the 0–200 Hz band, which are the main sources of noise inside the vehicle cabin.

6.5. Analysis of Ride Comfort at the Driver's Seat Under Sine Wave and Class C Random Road Profiles

The ride comfort at the driver's seat when the vehicle travels over a sine-wave road profile at 60 km/h is illustrated by the acceleration values at the driver's seat position, as shown in Fig. 14.

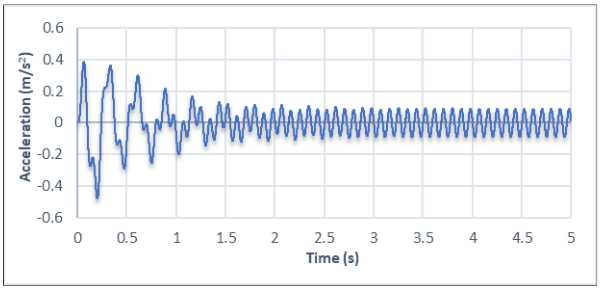

Fig. 14. Acceleration at the driver's position for a sine wave road surface

The ride comfort at the driver's seat under a class C random road profile according to ISO 8608:2016, at a vehicle speed of 60km/h, is represented by the acceleration values at the driver's seat position, as shown in Fig. 15.

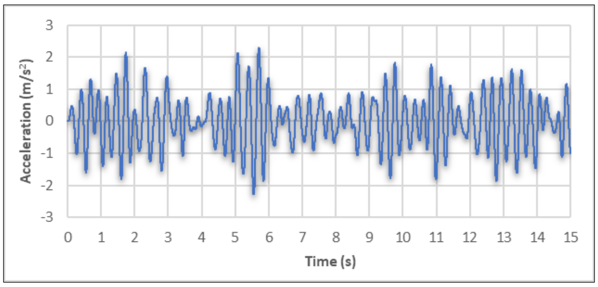

Fig. 15. Acceleration at the driver's seat with class C random road profile

The ISO 2631-1:1997/Amd 1:2010 standard is used to evaluate ride comfort at the driver's seat for two common road profiles in Vietnam. The investigated ride comfort metric is the root mean square acceleration value, denoted as a_{rms} (m/s^2).

The ride comfort metrics and driving conditions observed at the driver's seat are summarized in Table 11. At a vehicle speed of 60 km/h, the measured a_{rms} value on a sine wave road surface was 0.112 m/s². According to ISO 2631-1:1997/Amd 1:2010, this level falls below 0.315 m/s², corresponding to the not uncomfortable rating, indicating a high degree of ride comfort with minimal vibration exposure from the road. In contrast, when operating on a Class C random profile defined by ISO 8608:2016, the a_{rms} increased to 0.813 m/s², entering the uncomfortable range 0.8–1.6 m/s². This suggests that poorer road conditions generate significantly higher vibration levels, which can adversely impact passenger comfort. These findings highlight the necessity of optimizing seat and suspension systems to accommodate a wider range of road surfaces, or alternatively, managing driver exposure duration to maintain operational performance and long-term health.

Table 11. Evaluation of ride comfort at the driver's seat

Road surface profile	Speed (km/h)	a_{rms} (m/s^2)
Sine wave	60	0.112
Class C random road	60	0.813

7. CONCLUSION

The objective is to provide a more comprehensive understanding of the coupled structural–acoustic behavior under road surface excitation, thereby enabling a more accurate analysis of the sound transmission mechanisms and pressure field distribution at occupant seating locations. During the simulation process, to specifically evaluate the influence of vibrations from the road surface profile on the sound pressure level inside the vehicle cabin at various positions, other physical and technical conditions such as sound insulation systems, vehicle body airtightness, aerodynamic noise, tire noise, engine noise, etc., were completely eliminated. This simplification allowed the excitation source to be isolated solely to vibrations from road surface irregularities. It clarified the relationship between vibrations from the road profile through the suspension system, vehicle frame, and passenger compartment, and the variations in sound pressure inside the cabin. However, because energy dissipation and sound absorption mechanisms were not considered, the simulation results showed relatively high sound pressure levels, with peak values exceeding 190 dB for travel over a sine-wave road profile. For the case of a Class C random road profile according to ISO 8608:2016, the maximum SPL reached 138.61 dB. These are not the actual sound pressure levels experienced by occupants but idealized FEM model results under conditions without damping and with maximum simplifications to fit available computational resources. Therefore, these values should be considered as relative references, reflecting the trend of sound pressure distribution by location rather than directly indicating the real impact on drivers and passengers.

To supplement this assessment, vehicle ride comfort was also considered through the a_{rms} index. The results showed that for the sine wave road profile at 60 km/h, the comfort level corresponds to not uncomfortable according to occupant perception classification. Meanwhile, on the Class C random road surface, the a_{rms} value increased into the uncomfortable range. This distinction clearly demonstrates the influence of the road surface profile type not only on sound pressure levels but also on passenger comfort, as reflected in the mechanical vibrations transmitted into the vehicle cabin. Hence, the simulation results contribute not only to evaluating trends in acoustic variation but also provide a quantitative basis for studies on perceived ride comfort under idealized operating conditions.

CONFLICTS OF INTEREST

The author declares no conflict of interest.

REFERENCES

[1] J. Tatsuno, S. Maeda, Effect of Whole-Body Vibration Exposure in Vehicles on Static

Standing Balance after Riding. *Vibration*, 6(2), 2023: 343-358. https://doi.org/10.3390/vibration6020021

[2] H. Xue, G. Previati, M. Gobbi, G. Mastinu, Research and Development on Noise, Vibration, and Harshness of Road Vehicles Using Driving Simulators—A Review. *SAE International Journal of Vehicle Dynamics, Stability, and NVH*, 7(4), 2023: 555-577. https://doi.org/10.4271/10-07-04-0035

[3] ISO 8608:2016. Mechanical vibration — Road surface profiles — Reporting of measured data. *International Organization for Standardization*, Geneva, Switzerland, 2016. https://www.iso.org/standard/71202.html

[4] Z. Li, J. Li, Numerical Simulation Study of Aerodynamic Noise in High-Rise Buildings. *Applied Sciences*, 12(19), 2022: 9446. https://doi.org/10.3390/app12199446

[5] ISO 2631-1:1997/Amd 1:2010. Mechanical vibration and shock — Evaluation of human exposure to whole-body vibration — Part 1: General requirements. *International Organization for Standardization*, Geneva, Switzerland, 2010. https://www.iso.org/standard/7612.html

[6] R. Citarella, T. Landi, L. Caivano, G. D'Errico, F. Raffa, M. Romano, E. Armentani, Structural and Vibro-Acoustics Optimization of a Car Body Rear Part. *Applied Sciences*, 13(6), 2023: 3552. https://doi.org/10.3390/app13063552

[7] S. Xiao, J. He, G. Xu, Y. Li, Y. San, S. Cheng, Study on interior noise control of minibus based on structural acoustic radiation. *Proceedings of the Institution of Mechanical Engineers, Part D: Journal of Automobile Engineering*, 238(8), 2024: 2350-2367. https://doi.org/10.1177/09544070231163346

[8] Z. Zhang, Y. Zhang, C. Huang, X. Liu, Low-noise structure optimization of a heavy commercial vehicle cab based on approximation model. *Journal of Low Frequency Noise, Vibration and Active Control*, 37(4), 2018: 987-1002. https://doi.org/10.1177/1461348418798403

[9] M.D. Le, C.T. Le, T.T. Huynh, Control of noise in the passenger compartment of the bus due to structural vibration. *Proceedings of the Institution of Mechanical Engineers, Part D: Journal of Automobile Engineering*, 239(2-3), 2025: 984-1000. https://doi.org/10.1177/09544070231205360

[10] X. Cui, N. Zhai, Y. Cao, Simulation and Optimization of Bus Interior Noise Based on Hybrid Method for Engine Vibration Load Identification. *Shock and Vibration*, 2024(1), 2024: 9583817. https://doi.org/10.1155/2024/9583817

[11] Y. Wang, M. Du, C. Su, W. Wu, Numerical investigation on the contribution of underbody flow-induced noise on vehicle interior noise. *Proceedings of the Institution of Mechanical Engineers, Part D: Journal of Automobile Engineering*, 235(10-11), 2021: 2667-2678. https://doi.org/10.1177/09544070211004460

[12] T. Landi, C. Hoareau, J.-F. Deü, R. Ohayon, R. Citarella, Comparative vibroacoustic analyses: FEM vs. IGA. *Computational Mechanics*, 76, 2025: 1027-1059. https://doi.org/10.1007/s00466-025-02639-9

[13] J. Su, J. Lou, X. Jiang, Research on optimization control of vehicle road noise performance. *IOP Conference Series: Earth and Environmental Science*, 769(4), 2021: 042055. https://doi.org/10.1088/1755-1315/769/4/042055

[14] J. Frank, S. Doshi, M. Rao, P. Raghavendran, Reduction of driveline boom noise and vibration of 40 seat bus through structural optimization. *International Conference on Advances in Design, Materials, Manufacturing and Surface Engineering for Mobility*, July 19, 2017, Chennai, India. https://doi.org/10.4271/2017-28-1926

[15] D. Siano, M.A. Panza, Sound quality analysis of the powertrain booming noise in a Diesel passenger car. *Energy Procedia*, 126, 2017: 971-978. https://doi.org/10.1016/j.egypro.2017.08.189

[16] L. Gavric, NVH refinement issues for BEV. *Automotive Acoustics Conference 2019. Proceedings. Springer Vieweg*, 2019. https://doi.org/10.1007/978-3-658-27669-0_1

[17] F. Laib, A. Braun, W. Rid, Modelling noise reductions using electric buses in urban traffic. A case study from Stuttgart, Germany. *Transportation Research Procedia*, 37, 2019: 377-384. https://doi.org/10.1016/j.trpro.2018.12.206

[18] R.I. Rakhmatov, V.E Krutolapov, Development of vehicle noise-vibration-harshness analysis calculation method in order to improve NVH characteristics. *IOP Conference Series: Earth and Environmental Science*, 867, 2021: 012106. https://doi.org/10.1088/1755-1315/867/1/012106

[19] V.H. Quan, D.Q. Uy, Vehicle body vibration and noise impact on driver and passengers analysis: The case of the 29-seat Thaco Garden TB79s

bus. *Engineering, Technology & Applied Science Research*, 15(1), 2025: 20049-20055. https://doi.org/10.48084/etasr.9200

[20] N.A. Ngoc, L.H. Quan, V.H. Quan, N.M. Tien, N.N. Anh, Research on the Vibration of Passenger Car Using Magnetorheological Fluid Damper. *Proceedings of the 3rd Annual International Conference on Material, Machines and Methods for Sustainable Development (MMMS2022). Lecture Notes in Mechanical Engineering. Springer,* Cham, 2023, 377-383. https://doi.org/10.1007/978-3-031-31824-5_45

[21] S. Patil, G.U. Raju, C. Chavan, NVH Analysis of Car Cabin Compartment. *International Journal of Scientific Development and Research (IJSDR)*, 3(7), 2018: 317-324.

[22] S. Rao, A. Bhattu, Dynamic Analysis and Design Optimization of Automobile Chassis Frame Using FEM. In: Machines, Mechanism and Robotics. *Lecture Notes in Mechanical Engineering.* Springer, Singapore. 2019, 671-680. https://doi.org/10.1007/978-981-10-8597-0_57

[23] H. Xue, G. Fichera, M. Gobbi, G. Mastinu, G. Previati, D. Minen, Compact Full-Spectrum Driving Simulator Optimization for NVH Applications. *Vehicles*, 7(3), 2025: 66. https://doi.org/10.3390/vehicles7030066

[24] M. Li, S. Zhang, X. Zhang, M. Qiu, Z. Liu, S. He, Optimization Study of Driver Crash Injuries Considering the Body NVH Performance. *Applied Sciences*, 13(22), 2023: 12199. https://doi.org/10.3390/app132212199

[25] Z. Bai, J. Wei, K. Chen, Noise analysis of interior structure under powertrain excitation. *Journal of Physics: Conference Series*, 2691, 2024: 012019. https://doi.org/10.1088/1742-6596/2691/1/012019